Supplementary Figures

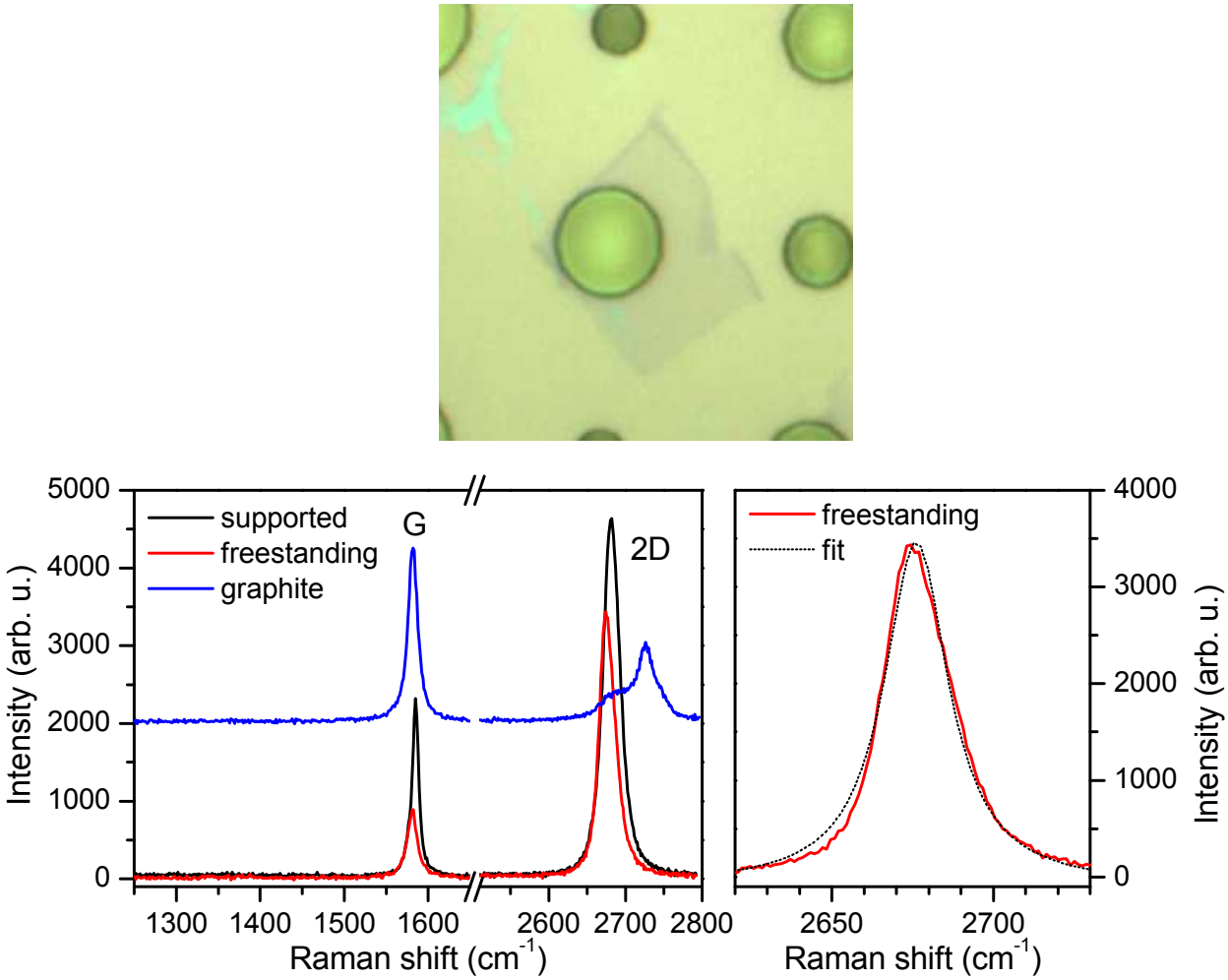

Figure S1. Raman spectra of freestanding graphene. Top, Optical micrograph of freestanding graphene (**F1**) suspended across a circular well (7 μm in diameter and 5 μm in depth). **Bottom left**, Raman spectra of freestanding graphene obtained from the center of the well in comparison with that obtained from the graphene area supported on the SiO_2 substrate. Raman spectrum of a thick graphite flake is also shown with an offset for clarity. (ω_G^0, ω_{2D}^0) of the freestanding region was found to be (1581.6 ± 0.2, 2676.9 ± 0.7) (cm^{-1}), while ω_G of graphite is 1581.5 ± 0.3 cm^{-1}. **Bottom right**, Expanded view of the 2D band of the freestanding graphene with a Lorentzian curve fit, which confirms the asymmetry first reported by Berciaud *et al*. (Ref. 34). Integration time for each Raman spectrum was 30 and 60 s for graphene and graphite, respectively.

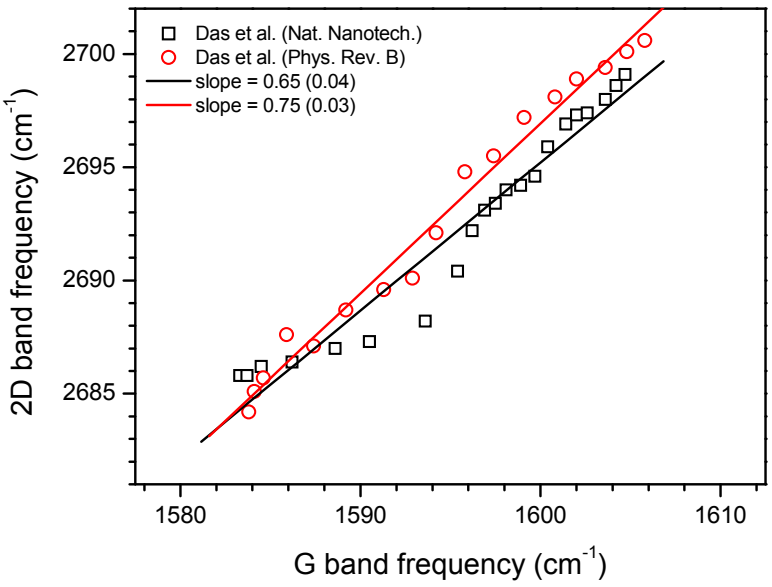

Figure S2. Correlation between ω_G and ω_{2D} of hole-doped graphene. The variation of 2D band frequency as a function of G band frequency for varying hole carrier density from 0 to ~2×10^{13} cm^{-2}. Data were extracted from previous works (Refs. 43 & 49). The solid lines are linear fits to each data set. The numbers in parentheses in the legend represent the fitting errors for the slopes. See Supplementary Methods A for details.

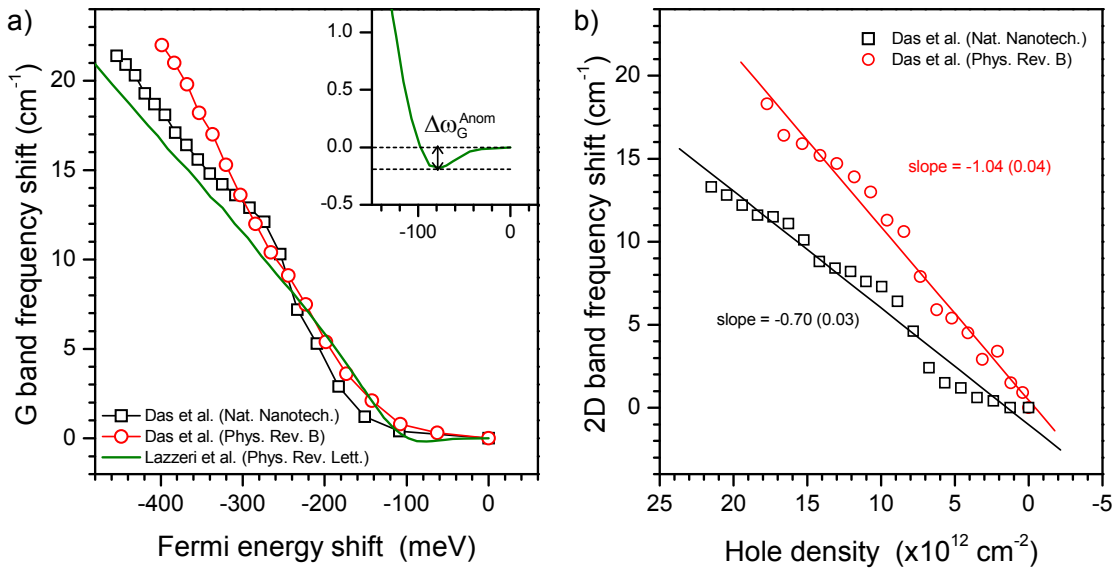

Figure S3. Effects of logarithmic phonon anomaly. a, The shifts of G band frequency ($\Delta\omega_G$) as a function of the Fermi energy shift: the black squares and red circles are experimental data and the green solid line is a theoretical calculation. The inset magnifies the low charge density region of the theoretical prediction. **b**, The shifts of 2D band frequency ($\Delta\omega_{2D}$) as a function of the hole density extracted from Das *et al.*'s works (Ref. 43 & 49). The solid lines are linear fits to the data. For consistency with the rest data sets, all the data from Ref. 43 in **a** and **b** were rescaled using the Fermi velocity of 0.839x10^6 m/s. See Supplementary Methods B for details.

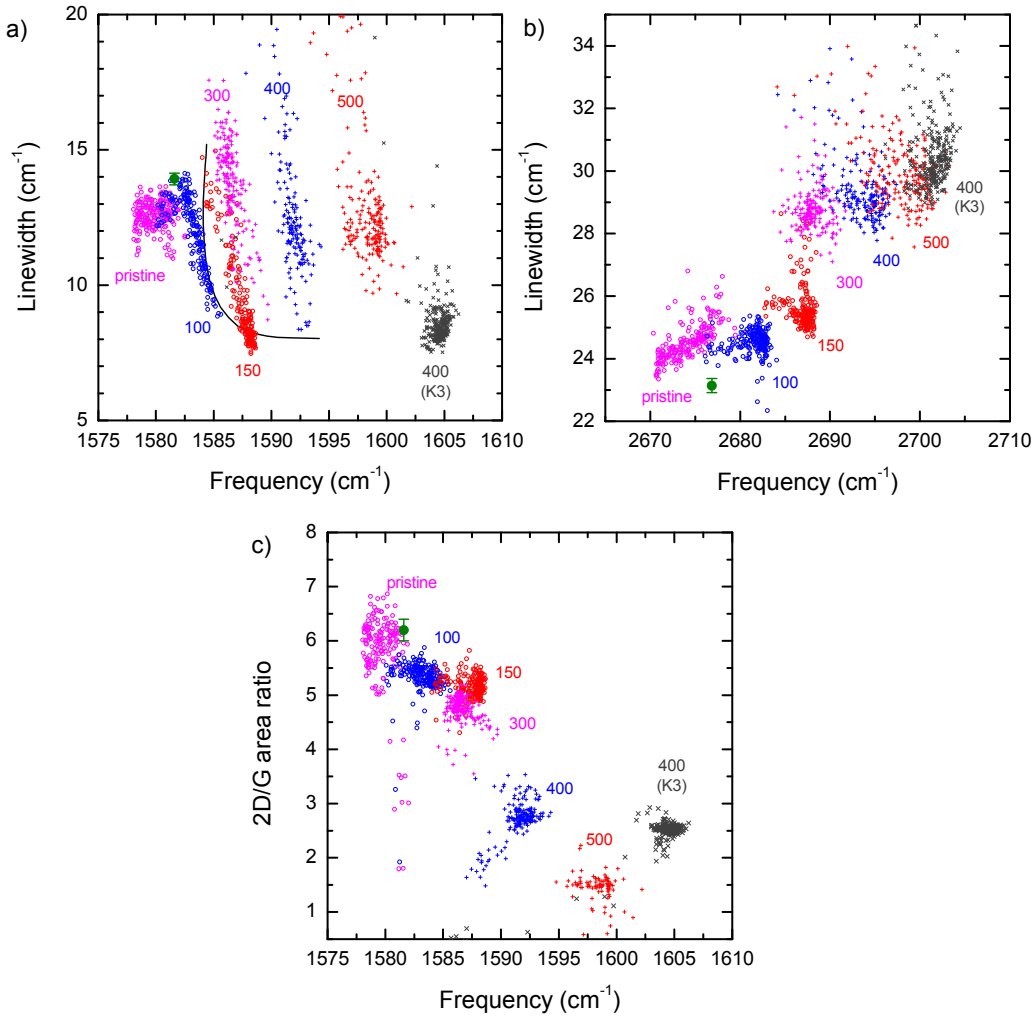

Figure S4. Annealing-induced changes in linewidths and 2D/G area ratio. Spectral variations in the G and 2D modes induced by successive thermal annealing. The data were extracted from the Raman measurements of **K4** given in Fig. 4. **a**, Correlation between linewidths (Γ_G) and frequencies (ω_G) of the G mode. **b**, Correlation between linewidths and frequencies of the 2D mode. **c**, Integrated area ratios between the 2D and G modes as a function of ω_G. The black line in **a** represents a theoretical prediction (Ref. 36) for Γ_G–ω_G affected by excess charges in graphene. The green circular dots with error bars in **a**~**c** were obtained from the freestanding graphene (**F1** in Fig. 2).

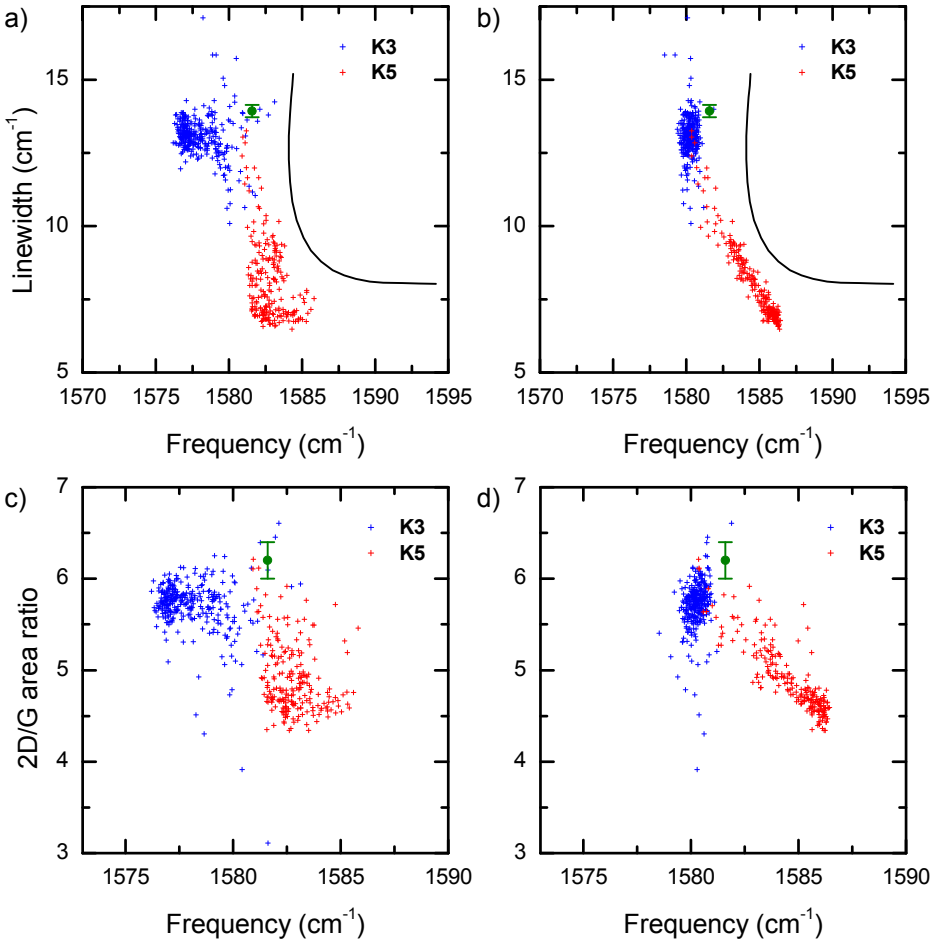

Figure S5. Spectral correlations enhanced by strain-correction. a, Correlation of the linewidths (Γ_G) and frequencies (ω_G) of the G mode for two pristine samples (**K3** & **K5**). **b**, The same data set as in **a**, but ω_G was replaced by $\omega_{G,\,\varepsilon=0}$ which was deduced from the vector analysis described in Fig. 5. The black lines in both graphs represent the theoretical prediction for Γ_G–ω_G affected by excess charges in graphene. (Ref. 36) **c**, Correlation of 2D/G area ratios and frequencies (ω_G) of the G mode for the two pristine samples (**K3** & **K5**). **d**, The same data set as in **c**, but ω_G was replaced by $\omega_{G,\,\varepsilon=0}$. The green circular dots with error bars in all panels were obtained from the freestanding graphene (**F1** in Fig. 2).

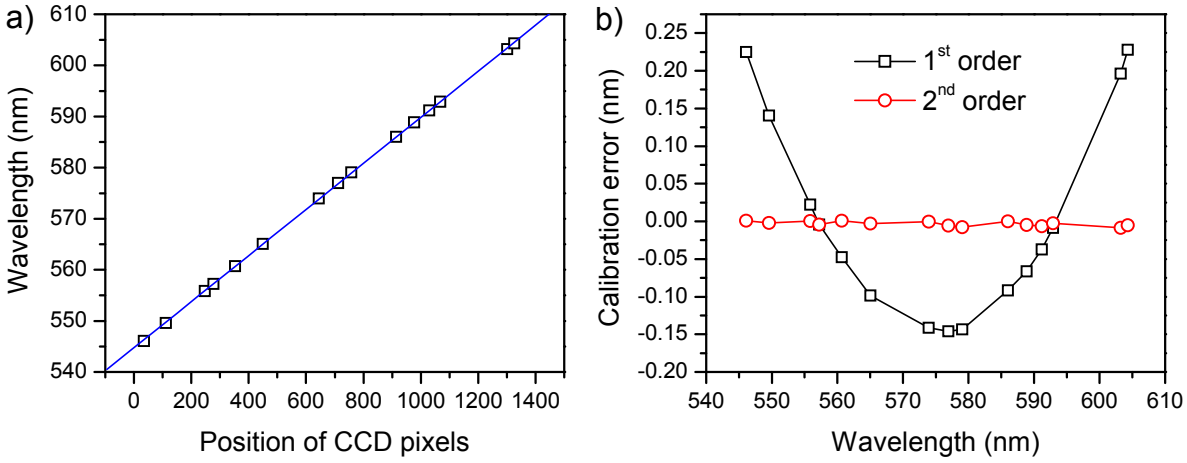

Figure S6. Spectral accuracy of the Raman measurements. a, Wavelengths of 3 Hg emission lines and 13 plasma lines of the Ar ion laser as a function of the position in the CCD detector. **b**, Calibration error in wavelength from the 1st and 2nd order calibrations, respectively. See Methods in the main text for details.

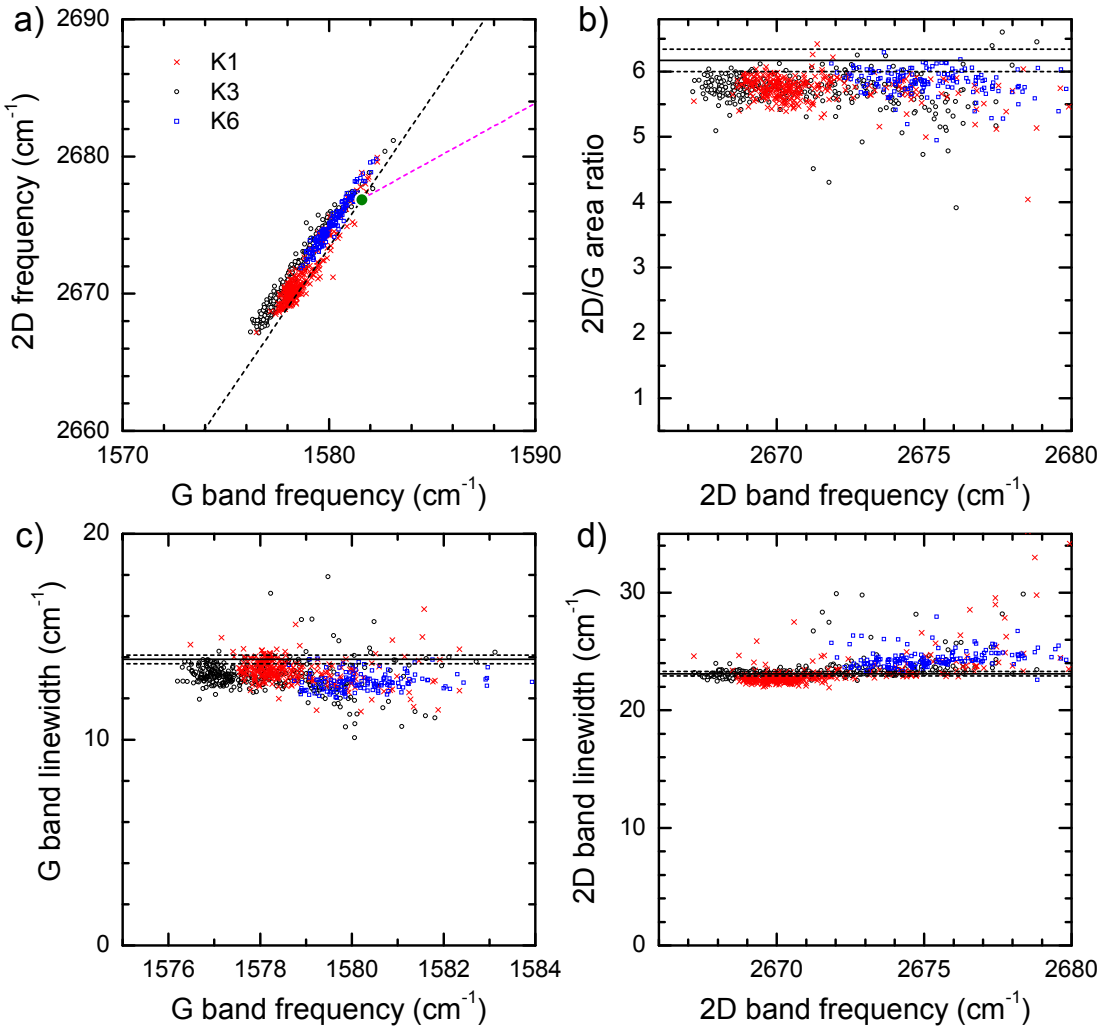

Figure S7. **Additional Raman spectral features of pristine graphene. a**, Correlation between the frequencies of the G and 2D Raman modes of pristine graphene (ω_G,ω_{2D}). **b**, 2D/G area ratio as a function of ω_{2D}. **c**, Γ_G as a function of ω_G. **d**, Γ_{2D} as a function of ω_{2D}. The solid and dashed lines in **b** ~ **d** represent, respectively, the average values and error ranges obtained from the freestanding graphene (**F1**). Each Raman spectrum of the map data was obtained for 15 s for **K1** & **K3**, and 10 s for **K6**. See Methods in the main text for details.

Supplementary Methods

A. Literature values for $\Delta\omega_{2D}/\Delta\omega_G$ caused by p-type charge doping

The effects of extra charge carriers on the G (ω_G) or 2D (ω_{2D}) band frequencies have been theoretically[35] and experimentally[32,33,43,46,49,60] well characterized. Das *et al*.[43] explained that ω_G and ω_{2D} increase (decrease) with increasing density of holes (electrons) assuming adiabatic electron-phonon coupling. For G mode, however, non-adiabatic coupling also needs to be considered, which leads to upshifts ω_G for both types of charges. In contrast, the non-adiabatic effects are thought to be negligible on 2D mode, resulting in asymmetric variation of ω_{2D} for both types of charges. Since the proposed vector analysis model requires the value of $\Delta\omega_{2D}/\Delta\omega_G$ for varying hole carrier density, we summarized experimental values[43,49] available in the literature in Supplementary Figure S2. (Yan *et al*.'s work[32] was not included since they did not report the numerical values for ω_{2D}.) By electrical gating, the hole carrier density was modulated up to ~2×10^{13} cm^{-2} which translates into ω_G = ~1605 cm^{-1} and ω_{2D} = ~2700 cm^{-1}. While the slopes corresponding to $\Delta\omega_{2D}/\Delta\omega_G$ are not completely constant and the two papers[43,49] reported by the same group lead to slightly different values, it can be seen that their variations are quasi-linear and agree with each other in the full range of hole density. As reference data for the effects of hole doping on ω_G and ω_{2D}, we used an average of the two results,[43,49] $(\Delta\omega_{2D}/\Delta\omega_G)_{\mathbf{n}}^{hole}$ = 0.70 ± 0.05. It should be noted, however, that the assumption of constant $(\Delta\omega_{2D}/\Delta\omega_G)_{\mathbf{n}}^{hole}$ is an approximation and more refined values of $\Delta\omega_{2D}/\Delta\omega_G$ for varying charge density will improve the accuracy of the proposed analysis.

B. Effects of logarithmic phonon anomaly at $|E_F| = \hbar\omega_G/2$

While the increase of ω_G is proportional to the shift of Fermi level in high charge carrier limit, Lazzeri *et al*.[35] predicted a phonon anomaly that G band softens logarithmically when $|E_F| = \hbar\omega_G/2$ (Supplementary Figure S3a.) The theory also predicts that the degree of the anomalous softening ($\delta\omega_G^{Anom}$, defined in the inset of Supplementary Figure S3a) will be larger at lower temperatures and less significant (~0.2 cm^{-1}) at 300 K. Yan *et al*.[46] confirmed the anomalous softening of G band for bilayer graphene but not for single layer graphene even at 12 K, and attributed its absence for single layer graphene to the native charge inhomogeneity and the fact that single layer graphene is more susceptible to E_F shift due to charge doping than bilayer. As shown in Supplementary Figure S3a, the two independent measurements[43,49] for single layer graphene at 300 K did not reveal noticeable softening as increasing the hole density ($\boldsymbol{n}$), which is consistent with the theory.[35] However, it is to be noted that while $\Delta\omega_G$, $\omega_G(\boldsymbol{n})$ - $\omega_G(0)$, is linearly proportional to $|\Delta E_F|$ in the high charge density limit ($|\Delta E_F|$ > 100 meV), it converges to zero at $|\Delta E_F|$ ~ 100 meV not 0 meV due to the phonon anomaly as decreasing $|\boldsymbol{n}|$.

As shown in Supplementary Figure S3b, the experimental values for $\Delta\omega_{2D}(\boldsymbol{n})$ defined as $\omega_{2D}(\boldsymbol{n})$ - $\omega_{2D}(0)$ show non-negligible discrepancy between the two available data sets,[43,49] while $\Delta\omega_{2D}$ shows a quasi-linear dependence on $\boldsymbol{n}$ for both. Since the theoretical work[35] did not provide $\Delta\omega_{2D}(\boldsymbol{n})$, the average of the experimental data in Supplementary Figure S3b were employed in plotting the blue solid line in Fig. 3a. The assumption of a linear relationship between $\Delta\omega_{2D}$ and $\boldsymbol{n}$ in Supplementary Figure S3b should be taken as an approximation which may be justified by the large disagreement in the available data. When reproducible experimental data and theoretical relationship between $\Delta\omega_{2D}$ and $\boldsymbol{n}$ become available, the accuracy of the proposed analytical method will be greatly improved.

C. Changes in linewidths and A_{2D}/A_G caused by stepwise annealing

The Lorentzian linewidths of G (Γ_G) and 2D (Γ_{2D}) peaks, and the 2D/G peak area ratios (A_{2D}/A_G) shown in Supplementary Figure S4 shed more light on the chemical and mechanical transformations caused by each annealing cycle. For the pristine graphene (**K4**), Γ_G and A_{2D}/A_G are 12.6 ± 0.5 cm^{-1} and 5.8 ± 0.8, respectively, where the uncertainty represents standard deviation for hundreds of data points for each data set. The values are close to those of the freestanding graphene (**F1**), Γ_G^0 = 13.9 ± 0.2 cm^{-1} and A_{2D}/A_G^0 = 6.2 ± 0.2. (Also note that Γ_G^0 of **F1** is in an excellent agreement with the previous observation by Berciaud *et al*.[34]) The slight decreases in the two parameters of **K4** are due to the substrate-mediated charge doping causing the blockage of the non-adiabatic decay channel of the G phonon[32] and decrease in the scattering cross section of the 2D Raman mode,[44] respectively, both of which are sensitive to very low level of charge doping.[34,43] Annealing at 100 ^oC further reduced Γ_G and A_{2D}/A_G with the data points largely complying with the theoretical prediction[43] on ω_G and Γ_G (solid line in Supplementary Figure S4a), indicating that extra charges are injected into graphene. While further annealing at higher temperatures decreased A_{2D}/A_G due to increasing hole density (Supplementary Figure S4c), however, Γ_G exhibited very broad distributions instead of obeying the theoretical prediction (solid line in Supplementary Figure S4a). We attribute the large spread in Γ_G of annealed **K4** to inhomogeneous broadening induced by the cycles of annealing treatments which should involve repeated compression-decompression of graphene. In fact, the sample **K3** that underwent the one-time annealing at 400 ^oC (Supplementary Figure S4a) shows decreased Γ_G with less spread despite its higher degree of charge doping. This was further confirmed in a control experiment where one sample (**K7**) was annealed for 12 hours at 400 ^oC and another (**K8**) underwent 6 cycles of 2 hour annealing at 400 ^oC. While Γ_G of one-time annealed **K7** was 8.7 ± 0.4 cm^{-1}, that of **K8** increased from 8.8 ± 0.3 cm^{-1} upon the first annealing to 15.8 ± 1.5 cm^{-1} upon the sixth annealing. Γ_{2D} of pristine **K4** was increased from ~24 cm^{-1} to ~30 cm^{-1} with noticeably increased spread when repeatedly annealed (Supplementary Figure S4b). The ~25 % increase in Γ_{2D} can be attributed to charge doping as was observed in the previous electrical gating experiment.[43]

D. Possibility of partial suspension of graphene on SiO_2 substrates

Despite the general notion that graphene largely conforms to underlying substrates due to its facile out-of-plane deformation,[18] there are experimental observations that some area of graphene on SiO_2 substrates can be considered as freestanding. Geringer *et al*.[22] showed that graphene is locally suspended between hills of underlying substrates generating intrinsic ripples.[61,62] Mashoff *et al*.[63] also revealed that nm-scale areas of graphene on SiO_2 substrates can be driven into high frequency oscillation along the out-of-plane direction suggesting the possibility of partial suspension or presence of intrinsic ripples. The presence of native strain, observed in the current study, will make such partial suspension of graphene more likely, since a graphene membrane under tensile stress would be stretched and suspended instead of conforming to the valley regions of the substrates when hung over hills. We also note that the Raman spectral features shown in Supplementary Figure S7, all indicating negligible charge doping, are consistent with the model of partially suspended graphene, since the native p-type doping in graphene on SiO_2 are generally believed to originate from the substrate itself[38,64,65] or occur through substrate-mediated mechanisms.[4,6,34]

E. Effects of optical interference on 2D/G peak area ratios (A_{2D}/A_G)

Yoon *et al*. showed that the optical media surrounding graphene affect the apparent 2D/G peak area ratio (A_{2D}/A_G) since the optical interference effects modulating the Raman intensities depend on the refractive indices of the media.[66] This means that A_{2D}/A_G of intrinsic graphene can be different when supported on substrates and freestanding in air. According to their calculation,[66] we find the following relationship for A_{2D}/A_G ratios for a few different substrates when excited by 514 nm laser:

$$(A_{2D}/A_G)_{\text{freestanding}} = 1.15(A_{2D}/A_G)_{285\text{ nm}} = 0.968(A_{2D}/A_G)_{300\text{ nm}} = 0.997(A_{2D}/A_G)_{\text{fused silica}} \quad \text{(S1)}$$

, where *freestanding* and *fused silica* indicates graphene suspended in air and supported on fused silica substrates, while *285 nm* and *300 nm* denote the thickness of underlying SiO_2 layer on top of Si substrates.

To exclude the purely optical effects, the observed 2D/G peak area ratio ($A_{2D}/A_G = 7.1 \pm 0.2$) of the freestanding graphene (**F1**) was converted for the case of graphene supported on 285 nm SiO_2/Si substrates using the above relationship. The resulting corrected value of **F1** ($A_{2D}/A_G^0 = 6.2 \pm 0.2$) was used for comparison with that of supported graphene.

Supplementary References

60 Casiraghi, C. Probing disorder and charged impurities in graphene by Raman spectroscopy. *Phys. Status Solidi-R.* **3**, 175-177 (2009).

61 Meyer, J. C. *et al.* The structure of suspended graphene sheets. *Nature* **446**, 60-63 (2007).

62 Fasolino, A., Los, J. H. & Katsnelson, M. I. Intrinsic ripples in graphene. *Nat. Mater.* **6**, 858-861 (2007).

63 Mashoff, T. *et al.* Bistability and oscillatory motion of natural nanomembranes appearing within monolayer graphene on silicon dioxide. *Nano Lett.* **10**, 461–465 (2010).

64 Romero, H. E. *et al.* N-type behavior of graphene supported on Si/SiO_2 substrates. *ACS Nano* **2**, 2037-2044 (2008).

65 Hossain, M. Z. Chemistry at the graphene-SiO_2 interface. *Appl. Phys. Lett.* **95**, 143125 (2009).

66 Yoon, D. *et al.* Interference effect on Raman spectrum of graphene on SiO_2/Si. *Phys. Rev. B* **80**, 125422 (2009).